A Memristor Device Model

Chris Yakopcic, *Student Member, IEEE*, Tarek M. Taha, *Member, IEEE*, Guru Subramanyam, *Senior Member, IEEE*, Robinson E. Pino, *Senior Member, IEEE*, and Stanley Rogers, *Member, IEEE*

***Abstract*—This letter proposes a new mathematical model for memristor devices. It builds on existing models and is correlated against several published device characterizations. This letter identifies significant discrepancies between the existing models and published device characterization data. The proposed model addresses these discrepancies. In particular, it allows modeling of memristor-based neuromorphic systems.**

***Index Terms*—Device model, memristive, memristor, simulation.**

I. Introduction

MEMRISTORS [1] were first discovered in 2008 [2]. Given that the dynamics of a memristor closely model a synapse [3], memristors are considered ideal for spiking-input-based neuromorphic systems. Thus, the simulation of memristors for spiking inputs is essential to the design of memristor-based neuromorphic systems. Physical devices reported in the literature [3]–[6] have been tested with sinusoidal inputs and zero-to-positive linearly increasing inputs. The behavior of the existing memristor models [2], [7], [8] for linearly increasing inputs is shown in [9]. Furthermore, Fig. 1 shows the simulation results for the model in [7] with a consecutively pulsed voltage input.

There are several discrepancies when comparing the results in Fig. 1 to the characterization data presented in [3]–[6]. The model results in Fig. 1 show that the size of the hysteresis loops in the positive regime increases as conductivity increases. When looking at the characterization data in [3]–[6], an opposite trend is present. Also, the memristor devices presented in [3]–[6] show a threshold voltage where hysteresis is not seen unless the voltage across the memristor exceeds the threshold. No threshold voltage is present in the existing models [2], [7], [8]. Lastly, Pickett *et al.* at HP Labs published characterization data where the motion of the state variable depends on both its value and the polarity of the applied current [10]. Previous models show the motion of the state variable to be equivalent, whether it is moving in the positive or negative direction. The value of the state variable represents the change in the physical properties of the memristor that is inversely proportional to the resistance.

Manuscript received May 3, 2011; revised July 7, 2011; accepted July 7, 2011. Date of publication September 7, 2011; date of current version September 28, 2011. The review of this letter was arranged by Editor A. Ortiz-Conde.

C. Yakopcic, T. M. Taha, and G. Subramanyam are with the University of Dayton, Dayton, OH 45469 USA (e-mail: yakopccg@notes.udayton.edu; tarek.taha@notes.udayton.edu; guru.subramanyam@notes.udayton.edu).

R. E. Pino is with the Air Force Research Laboratory, Rome, NY 13441 USA (e-mail: Robinson.Pino@rl.af.mil).

S. Rogers is with the Air Force Research Laboratory, Wright-Patterson Air Force Base, OH 45433 USA (e-mail: Stanley.Rogers2@wpafb.af.mil).

Color versions of one or more of the figures in this letter are available online at http://ieeexplore.ieee.org.

Digital Object Identifier 10.1109/LED.2011.2163292

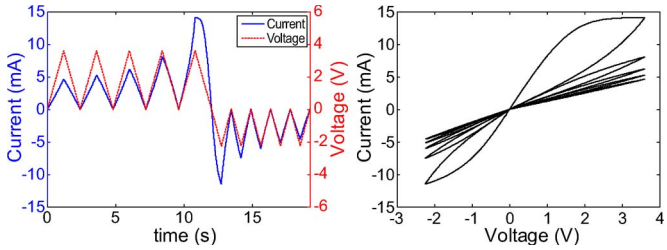

Fig. 1. Simulated I–V characteristic using the memristor model in [7].

This letter proposes a model that is able to capture device responses for linearly increasing and sinusoidal inputs. The model was developed based on an I–V relationship proposed in [11] and a switching state variable similar to the one in [10]. The model was correlated to the I–V data of memristor devices published by HP Labs [3], [4] (TiO_2), the University of Michigan [5] (a-Si and Ag), and Boise State University [6] (Ag chalcogenide). Due to the large variation in memristor device structure and operation, the model uses many fitting parameters to simulate the effects of the different devices. The model has not yet been tested for its validity with other memristive devices such as spintronic memristors [12], RRAM devices [13], or phase change memory [14]. A model was developed in [15] based on the modulation of a metal–insulator–metal (MIM) tunnel barrier that provides a strong correlation to physical device data, although it appears to only be valid for TiO_2-based devices. Furthermore, the model in [15] was not tested using consecutive zero-to-positive sweeping inputs. The model presented in this letter can be used to provide accurate circuit simulations and power analysis for a wide range of memristor devices and voltage inputs.

II. Proposed Memristor Model

The I–V relationship for the memristor model can be seen in (1) and was previously proposed in [11]. The hyperbolic sinusoid shape is due to the MIM structure of memristors [16]. The MIM structure causes the device to have an increase in conductivity beyond a certain voltage threshold. The parameters a_1, a_2, and b are used to fit (1) to the different device structures of the memristors studied in this letter. Based on existing memristor characterization data, the devices appear to be more conductive when they are positively biased. To account for this, a different amplitude parameter is required depending on the polarity of the input voltage. The fitting parameter b was used to control the intensity of the threshold function relating conductivity to input voltage magnitude. For example, the device published in [3] has a stronger threshold ($b = 3$) than the device published in [5]($b = 0.7$). The I–V relationship also depends on the state variable $x(t)$, which provides the change in resistance based on the physical dynamics in each device.

In this model, the state variable is a value between zero and one that directly impacts the conductivity of the device

$$I(t) = \begin{cases} a_1 x(t) \sinh\left(bV(t)\right), & V(t) \geq 0 \\ a_2 x(t) \sinh\left(bV(t)\right), & V(t) < 0. \end{cases} \tag{1}$$

The change in the state variable is based on two different functions, namely, $g(V(t))$ and $f(x(t))$. The function $g(V(t))$ imposes a programming threshold on the memristor model. Each of the published memristor devices [3]–[6] shows that there is no state change in the memristor unless a certain voltage threshold is exceeded. The threshold is viewed as the minimum energy required to impose a change on the physical structure of the device. These changes include the motion of low-mobility ions or dopants [3]–[5] or the state change in a chalcogenide device [6]. The programming threshold was implemented using (2). As opposed to the hyperbolic sinusoid programming threshold implemented in [11], the method in (2) provides the possibility of having different thresholds based on the polarity of the input voltage. This is required to provide a better fit to the characterization data since several of these devices show different threshold values, depending on whether the input voltage is positive or negative.

In addition to the positive and negative thresholds (V_p and V_n), the magnitude of the exponentials (A_p and A_n) can be adjusted. These magnitudes represent how quickly the state changes once the threshold is surpassed. In the results hereinafter, it can be seen that the chalcogenide device [6] requires a very large change once the threshold is surpassed. Alternatively, the device based on the motion of silver dopants [5] requires a much lower amplitude coefficient as this appears to be a slower phenomenon

$$g\left(V(t)\right) = \begin{cases} A_p\left(e^{V(t)} - e^{V_p}\right), & V(t) > V_p \\ -A_n\left(e^{-V(t)} - e^{V_n}\right), & V(t) < -V_n \\ 0, & -V_n \leq V(t) \leq V_p. \end{cases} \tag{2}$$

The second function, used to model the state variable $f(x(t))$, can be seen in (3) and (4). This function was added based on the assumption that it becomes harder to change the state of the devices as the state variable approaches the boundaries. This idea was theorized in [7] and [8] and determined experimentally in [10]. Also, this function provides the possibility of modeling the motion of the state variable differently depending on the polarity of the input voltage. This technique was first used in [10] to develop a different state variable equation that is also dependent on the polarity of the input signal. One possible explanation for this may be that it is more difficult to put ions back in their original position after they have been previously removed. When $V(t) > 0$, the state variable motion is described by (3); otherwise, the motion is described by (4).

The function $f(x(t))$ was developed assuming that the state variable motion was constant up until the point x_p or x_n. At this point, the motion of the state variable was limited by a decaying exponential function. Since the motion of the state variable appears to be different across the different types of devices studied, this function used fitting parameters to accommodate the variety. The constants in this equation represent the point where the state variable motion becomes limited (x_p and x_n) and the rate at which the exponential decays (α_n and α_p). These differences may be due to the fact that the motion of the state change in a chalcogenide device is very different than the motion of ions or dopants

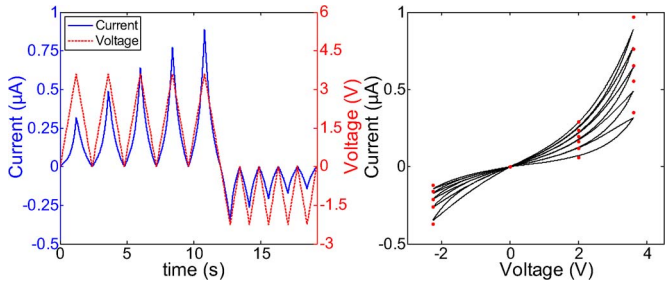

Fig. 2. Results obtained for matching characterization in [5]. Dots show the points from [5]. In this simulation, $V_p = 1.5$ V, $V_n = 0.5$ V, $A_p = 0.005$, $A_n = 0.08$, $x_p = 0.2$, $x_n = 0.5$, $\alpha_p = 1.2$, $\alpha_n = 3$, $a_1 = 3.7(10^{-7})$, $a_2 = 4.35(10^{-7})$, $b = 0.7$, and $x_0 = 0.1$.

$$f(x) = \begin{cases} e^{-\alpha_p(x - x_p)} w_p(x, x_p), & x \geq x_p \\ 1, & x < x_p \end{cases} \tag{3}$$

$$f(x) = \begin{cases} e^{\alpha_n(x + x_n - 1)} w_n(x, x_n), & x \leq 1 - x_n \\ 1, & x > 1 - x_n. \end{cases} \tag{4}$$

In (5), $w_p(x, x_p)$ is a windowing function that ensures that $f(x)$ equals zero when $x(t) = 1$ and $V(t) > 0$. In (6), $w_n(x, x_n)$ keeps $x(t)$ from becoming less than zero when the current flow is reversed

$$w_p(x, x_p) = \frac{x_p - x}{1 - x_p} + 1 \tag{5}$$

$$w_n(x, x_n) = \frac{x}{1 - x_n}. \tag{6}$$

Equation (7) is used to model the state variable motion in each of the memristor devices. Since the modeled state variable must match devices with many different physical structures, this equation is very different than the equation in [2] that was used to model only TiO_2 devices

$$\frac{dx}{dt} = g\left(V(t)\right) f\left(x(t)\right). \tag{7}$$

III. Device Simulations

The equations in the previous section were evaluated in MATLAB and applied to the different published memristor devices [3]–[6]. Fig. 2 shows the simulation results along with dots that correspond to selected points from the I–V characteristic in [5]. The simulation matches each target data point with an average error of 20.0 nA (6.21%). The percent error was determined by using the sum of the error divided by the absolute sum of the currents at each of the tested points.

Fig. 3 shows the results when simulating the device published in [6] with an average error of 32.7 μA (6.66%). No data were provided for negative dc sweeps in [6], so modeling parameters were assumed that caused the negative current peaks to match the general pattern for the other devices.

The simulation results based on the characterization data from HP Labs [3], [4] are displayed for both a multiple dc sweep input (Fig. 4) and a cyclical voltage sweep (Fig. 5) with an average error of 1.89 μA (11.66%) and 8.63 μA (13.6%), respectively. The error for the cyclical sweep dropped to 8.72% when not considering the largest outlier.

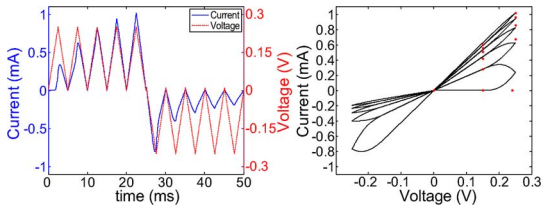

Fig. 3. Results obtained for matching characterization in [6]. Dots show the points from [6]. In this simulation, $V_p = 0.16$ V, $V_n = 0.15$ V, $A_p = 4000$, $A_n = 4000$, $x_p = 0.3$, $x_n = 0.5$, $\alpha_p = 1$, $\alpha_n = 5$, $a_1 = 0.097$, $a_2 = 0.097$, $b = 0.05$, and $x_0 = 0.001$.

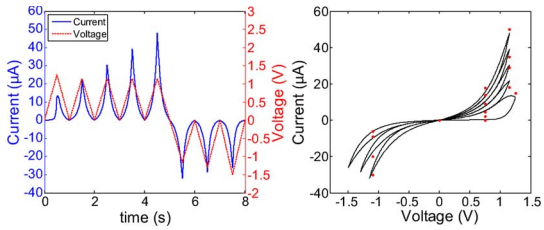

Fig. 4. Results obtained for matching characterization in [3]. Dots show the points from [3]. In this simulation, $V_p = 0.9$ V, $V_n = 0.2$ V, $A_p = 0.1$, $A_n = 10$, $x_p = 0.15$, $x_n = 0.25$, $\alpha_p = 1$, $\alpha_n = 4$, $a_1 = 0.076$, $a_2 = 0.06$, $b = 3$, and $x_0 = 0.001$.

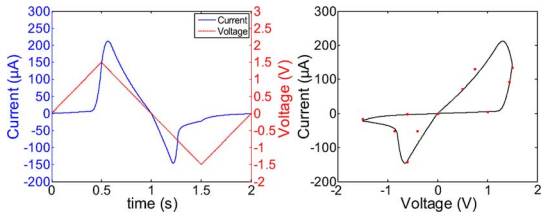

Fig. 5. Simulation results for the device in [4] for a circular dc sweep (dots show target data points). $V_p = 1.2$ V, $V_n = 0.6$ V, $A_p = 5$, $A_n = 30$, $x_p = 0.7$, $x_n = 0.8$, $\alpha_p = 4$, $\alpha_n = 24$, $a_1 = 2.3(10^{-4})$, $a_2 = 3.8(10^{-4})$, $b = 1$, and $x_0 = 0.02$.

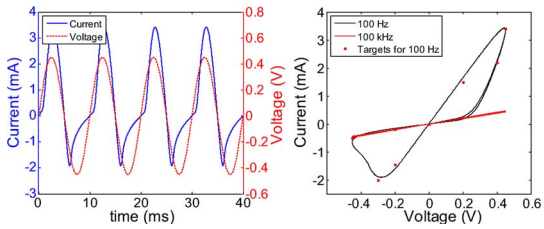

Fig. 6. Simulation results for the device in [6] for a sinusoidal input (dots show target data points). In this simulation, $V_p = 0.16$ V, $V_n = 0.15$ V, $A_p = 4000$, $A_n = 4000$, $x_p = 0.3$, $x_n = 0.5$, $\alpha_p = 1$, $\alpha_n = 5$, $a_1 = 0.17$, $a_2 = 0.17$, $b = 0.05$, and $x_0 = 0.11$.

Fig. 6 shows the simulation results when modeling the device in [6] using a sinusoidal input with an average error of 84.8 μA (6.64%). The hysteresis in the model diminished when the frequency was increased to 100 kHz just as it did in [6].

A number of insights emerged when comparing the different device models. The model developed in [15] suggests that the TiO_2 device has a dynamic resistance due to the modulation of a tunnel barrier in a MIM junction. Due to the curvature and similar threshold values (V_p and V_n) of the device in [5], it is possible that this device may also have dynamics provided by a tunnel barrier modulation in the Ag-poor region. The significantly lower conductivity multipliers (a_1 and a_2) could be explained by a barrier with a larger average thickness. When looking at the parameters representing exponential decay of state variable motion, it can be seen that α_n is more than double the value of α_p in each case. This is most likely caused by the reduction in conductivity due to a decreasing state variable, in addition to the reduction of motion near the boundaries, resulting in a larger rate of decay. Lastly, it would appear that the chalcogenide-based device has significantly lower programming thresholds (V_p and V_n) than the devices based on migration. This is balanced by the fact that the chalcogenide device also has the highest conductivity multipliers (a_1 and a_2), so the low programming threshold does not necessarily make it more energy efficient than the other devices.

IV. Conclusion

A device model for the memristor has been developed based on previous modeling techniques [10], [11], [15] that shows a close match to several published memristor devices. Adjusting the fitting parameters provided the capability of simulating devices with different physical structures. Given that neural spikes are more similar to linearly increasing zero-to-positive dc sweeps than to sinusoidal inputs, accurate modeling of dc sweep performance is important for neuromorphic systems. The model presented is able to simulate behavior for both types of inputs.

References

[1] L. O. Chua and O. Leon, "Memristor—The missing circuit element," *IEEE Trans. Circuit Theory*, vol. CT-18, no. 5, pp. 507–519, Sep. 1971.
[2] D. B. Strukov, G. S. Snider, D. R. Stewart, and R. S. Williams, "The missing memristor found," *Nature*, vol. 453, no. 7191, pp. 80–83, 2008.
[3] G. S. Snider, "Cortical computing with memristive nanodevices," SciDAC Rev., Washington, DC, 2008.
[4] J. J. Yang, M. D. Pickett, X. Li, D. A. A. Ohlberg, D. R. Stewart, and R. S. Williams, "Memristive switching mechanism for metal/oxide/metal nanodevices," *Nat. Nanotechnol.*, vol. 3, no. 7, pp. 429–433, Jul. 2008.
[5] S. H. Jo, T. Chang, I. Ebong, B. B. Bhadviya, P. Mazumder, and W. Lu, "Nanoscale memristor device as synapse in neuromorphic systems," *Nano Lett.*, vol. 10, no. 4, pp. 1297–1301, Apr. 2010.
[6] A. S. Oblea, A. Timilsina, D. Moore, and K. A. Campbell, "Silver chalcogenide based memristor devices," in *Proc. IJCNN*, 2010, pp. 1–3.
[7] Z. Biolek, D. Biolek, and V. Biolková, "Spice model of memristor with nonlinear dopant drift," *Radioengineering*, vol. 18, no. 2, pp. 210–214, 2009.
[8] Y. N. Joglekar and S. J. Wolf, "The elusive memristor: Properties of basic electrical circuits," *Eur. J. Phys.*, vol. 30, no. 4, p. 661, Jul. 2009.
[9] C. Yakopcic, T. M. Taha, G. Subramanyam, E. Shin, P. T. Murray, and S. Rogers, "Memristor-based pattern recognition for image processing: An adaptive coded aperture imaging and sensing opportunity," in *Proc. SPIE Adaptive Coded Aperture Imag. Non-Imag. Sens.*, 2010, vol. 7818, p. 78180E.
[10] M. D. Pickett, D. B. Strukov, J. L. Borghetti, J. J. Yang, G. S. Snider, D. R. Stewart, and R. S. Williams, "Switching dynamics in titanium dioxide memristive devices," *J. Appl. Phys.*, vol. 106, no. 7, p. 074 508, Oct. 2009.
[11] M. Laiho, E. Lehtonen, A. Russel, and P. Dudek, "Memristive synapses are becoming a reality," *The Neuromorphic Engineer*. College Park, MD: Inst. Neuromorphic Eng., 2010.
[12] X. Wang, Y. Chen, H. Xi, H. Li, and D. Diminov, "Spintronic memristor through spin-torque-induced magnetization motion," *IEEE Electron Device Lett.*, vol. 30, no. 3, pp. 294–297, Mar. 2009.
[13] K. W. Zhang, S. B. Long, Q. Liu, H. B. Lu, Y. T. Li, Y. Wang, W. T. Lian, M. Wang, S. Zhang, and M. Liu, "Progress in rectifying-based RRAM passive crossbar array," *Sci. China Technol. Sci.*, vol. 54, no. 4, pp. 811–818, Apr. 2011.
[14] H. P. Wong, S. Raoux, S. Kim, J. Liang, J. P. Reifenberg, B. Rajendran, M. Asheghi, and K. E. Goodson, "Phase change memory," *Proc. IEEE*, vol. 98, no. 12, pp. 2201–2227, Dec. 2010.
[15] H. Abdalla and M. D. Pickett, "SPICE modeling of memristors," in *Proc. ISCAS*, 2011, pp. 1832–1835.
[16] J. G. Simmons, "Generalized formula for the electric tunnel effect between similar electrodes separated by a thin insulating film," *J. Appl. Phys.*, vol. 34, no. 6, p. 1793, Jun. 1963.